Biosensors and Bioelectronics 37 (2012) 30–37

Contents lists available at SciVerse ScienceDirect

Biosensors and Bioelectronics

journal homepage: www.elsevier.com/locate/bios

Modulating electron transfer properties of gold nanoparticles for efficient biosensing

Shikha Sharma, Nidhi Gupta, Sudha Srivastava *

Department of biotechnology, Jaypee Institute of Information Technology, Noida, UP-201307, India

ARTICLE INFO

Article history:
Received 13 January 2012
Received in revised form
28 March 2012
Accepted 16 April 2012
Available online 3 May 2012

Keywords:
Glucose biosensor
Glucose oxidase
L-Serine
Coupled gold nanoparticles

ABSTRACT

Present study concerns modulating the electron transfer properties of gold nanoparticles through amino acid induced coupling among them. In addition to conductivity, the amino functionalization of the nanoparticles results in enhanced activity and operational stability of the biosensor fabricated using the same. Nanoparticles synthesized using amino acid as reducing agent (average diameter—20 nm), incorporate the natural coupling property of amino acids and are seen to align in a chain-like arrangement. The coupling of the individual nanoparticles to form chain like structure was confirmed by both absorption spectroscopy as well as transmission electron microscopy. The glucose biosensor developed by adsorption of glucose oxidase (GOx) enzyme onto these coupled gold nanoparticles showed enhanced efficiency as compared to the one with glucose oxidase immobilized onto gold nanoparticles synthesized using the conventional method (trisodium citrate as reducing agent). The fabricated biosensor demonstrated a wide linear concentration range from 1 μM–5 mM and a high sensitivity of 47.2 μA mM^{-1} cm^{-2}. Also, an enhanced selectivity to glucose was observed with negligible interference in the physiological range, from easily oxidizable biospecies, e.g. uric acid and ascorbic acid. Furthermore, the electrochemical biosensor has excellent long term stability- retaining greater than 85% of the biosensor activity up to 60 days.

1. Introduction

Glucose biosensors continues to remain in the forefront on account of two different research interests—one being its wide commercial applicability (ranging from chemical (Mao et al., 2008), pharmaceutical (Medyantev et al., 2008), food (Pmiertu et al., 1998), beverages to medicine (Zeng et al., 2011)) while the other is geared towards improvising the performance of the biosensors to targeted industrial applications. The need of the hour is to develop biosensor with wide linear range, high sensitivity and operational stability, in addition to reduced response time. Since the pioneering work of Clark and Lyons (1962), development in biosensor performance has undergone tremendous change and hence they are categorized as first-, second- and third generation biosensors with reduction in response time from 30 min to 100 s. With the advent of nano-technology, the response time of various biosensors – amperometric (Periasamy et al., 2011; Miao et al., 2011), potentiometric (Fernandez et al., 2008; Liao et al., 2007), optical (Prabhakar et al., 2008; Choi et al., 2001) and piezoelectric (Wang et al., 2009), could further be reduced to a few seconds.

Amperometric glucose biosensors based on gold (Ren et al., 2009), magnetic (Zuo et al., 2008), silica (Zhang et al., 2004), platinum (Cao et al., 2007), nickel (Wang et al., 2010), silver (Shi and Ma., 2010) and carbon nanotubes (Nenkova et al., 2010), graphene (Shan et al., 2009) have been developed and a reduction in response time from ~100 s to as low as 4–6 s have been achieved. These biosensors witnessed a progressive enhancement in sensitivity from 2 to 60 μA mM^{-1} cm^{-2}, however, the linear range decreased remarkably with increased sensitivity (as evident from Table 1). In addition to this, the stability of the reported biosensors was at best 80% up to 45 days. Therefore, the development of highly selective, sensitive and stable glucose biosensor is still imperatively needed.

In the present paper, the focus is on modulating the electron transfer properties of gold nanoparticles by inducing coupling amongst the particles. Gold nanoparticles attached in the form of a chain were synthesized using L-Serine, an amino acid, as a reducing and capping agent. Usage of the above amino acid facilitates the coupling among the particles (the chain like arrangement of particles). The glucose biosensor developed by immobilization of glucose oxidase enzyme onto amino functionalized chain like coupled gold nanoparticles showed an enhanced sensitivity of 47.2 μA mM^{-1} cm^{-2}, excellent operational stability, i.e., more than 85% up to two months, wide linear range from 1 μM to 5 mM and the selectivity was also very good with no interference from ascorbic acid and uric acid (in the physiological range).

* Corresponding author. Tel.: +91 120 2594213; fax: +91 120 2400986.
E-mail address: sudha.srivastava@jiit.ac.in (S. Srivastava).

0956-5663/$ - see front matter © 2012 Elsevier B.V. All rights reserved.
http://dx.doi.org/10.1016/j.bios.2012.04.027

Table 1
Performance of some of the reported glucose biosensors based on their immobilization support and sensitivity and stability parameters.

Type	Type of support for Immobilization	Sensitivity ($\mu A\ mM^{-1}\ cm^{-2}$)	Interference (physiological range of UA, mM and AA, mM)	Detection limit (μM)	Linear range (mM)	Response time (s)	Storage stability	Reference
Amperometric	Present work	47.2	No interference with concentration similar to physiological fluid, Non-interferring up to 1.36 mM (24.6 mg/dL) and uric acid up to 0.5 mM (9 mg/dL)	1.0	0.001–5	4	15% decrease in 60 days	Present work
Amperometric	Poly(3,4-ethylenedioxythiophene) film	12.42	With ascorbic acid current increases 9.7% and with uric acid 39.1%.	130.0	0.1–10	4–10	20% decrease after 18 days	Nien et al. (2006)
Amperometric	Layered double hydroxides (LDHs)	60	Negligible	3	0.0067–0.386	5	–	Shan et al. (2007)
Amperometric	Exfoliated graphite nanoplatelets Nafion membrane	14.17	Current enhancement, 56.8% for 0.1 mM ascorbic acid and 125% for 0.2 mM uric acid interference	10	up to 6	5	Stability for 7 days	Lu et al. (2007)
Amperometric	Amino functionalized multi-wall carbon nanotubes (MWNTs)	7.46	Minimum interference	8.0	–	<10	–	Sun et al. (2008)
Amperometric	Single walled carbon nanohorns	15.0	Can avoid the commonly coexisted interference	6.0	0–6	–	–	Liu et al. (2008)
Amperometric	Aminated silica nanoparticles	5.11	–	9.0	Up to 8	4	90% decrease in 45 days	Sun et al. (2006)
Amperometric	Graphene	–	–	–	2–14	–	–	Shan et al. (2009)
Amperometric	Poly (3,4-ethylenedioxythiophene)/ Prussian blue bilayer and multi-walled carbon nanotubes	2.67	–	–	1–10	–	18% decrease in 30 days	Chiu et al. (2009)
Amperometric	Platinum nanoparticles/ graphene/chitosan nanocomposite film	–	Negligible (with concentration similar to physiological fluid)	0.6	sub μM–5 mM	–	25% decrease in 14 days	Wu et al. (2009)
Amperometric	Gold nanorods/cellulose acetate composite film	8.4	–	20	0.03–2.2	–	20% decrease in 30 days	Ren et al. (2009)
Amperometric	Palladium nanoparticles/ chitosan-grafted graphene nanocomposites	31.2	Significant interference with concentration similar to physiological fluid at working potential of 0.7 V	0.2	0.001–1.0	–	20% decrease in 21 days	Zeng et al. (2011)

2. Experimental

2.1. Reagents and apparatus

Glucose oxidase (GOx, extracted from Aspergillus niger), Peroxidase enzyme, Gold (III) chloride trihydrate, cystamine dihydrochloride and D(+)-Glucose were purchased from Sigma-Aldrich Chemicals whereas L-Serine, Glutaraldehyde, Acetic acid, Potassium Dihydrogen phosphate and Potassium Hydrogen phosphate, Phenol, 4-Amino Anti Pyrine (4-AAP), and other chemicals were obtained from CDH. All glassware were cleaned in aqua regia and further rinsed with double distilled water thoroughly before use. The stock solution of GOx was prepared in PBS buffer and stored at 4 °C. A stock solution of D-glucose (2.0%) was prepared and allowed to mutarotate at room temperature for 24 h before measurements. Molecular biology grade (Hyclone) water was used for preparing all the reagents, so as to avoid background conductivity from water sample itself.

The electrochemical experiments were performed using a screen printed 3-electrode system (DRP550; Drop Sens), with a modified working (Pt) electrode as cathode, a counter electrode (Pt) and silver electrode as the reference (anode). A microammeter was connected in series with the working electrode to measure the current. The current response was measured as a function of glucose concentration at a constant applied voltage. Response time was calculated as the time required to sense 95% change in concentration. The cyclic voltammogram experiments employing the biosensors constructed were carried out using a computer-controlled Electrochemical Analyzer (Autolab, Netherlands). The electrochemical impedance measurements of nanoparticle solutions were performed using 3522-50 LCR HiTESTER (HIOKI) and the results were plotted in the form of complex impedance plane plots (Cole–Cole plots) with a frequency range from 10 Hz to 100 kHz. The potential of the system was set at 0.1 V. JEOL 2100F transmission electron microscope was used for the particle size estimation and the optical properties of nanoparticles were assessed ND 1000 UV–vis Spectrophotometer (Nanodrop technologies) operated at 12 V.

2.2. Gold nanoparticles (NPs) synthesis

Gold nanoparticles were synthesized by reduction of chloroauric acid using two approaches – (a) the conventional method (75 mM sodium citrate as reducing agent)(Turkevich et al., 1951) and (b) an amino acid as reducing agent (Tan et al., 2008; Majzik et al., 2010) (as shown in Fig. S1 in Supplementary Material). The latter protocol consists of adding 2 mL of 5 mM chloroauric acid to 100 ml of deionized water heated to boiling point. To the boiling mixture 3 ml of 75 mM L-Serine was added at a constant flow rate. Within few seconds the color of the solution turned to pale red indicating the commencement of colloidal gold formation. Heating and stirring was continued until the solution turned bright red and then it was quenched using an ice bath. This was followed by sonication for 15 min in an ultrasonicator water bath. Mixtures were then thermalized to room temperature and a pinkish red colored colloidal solution was observed. The colloidal solutions thus formed were centrifuged at 9000 rpm for 30 min. The pellet containing the amino functionalized gold nanoparticles were stored at room temperature till further processing.

2.3. Fabrication of GOx–Pt, GOx–Au citrate NPs–Pt and GOx–Au amino NPs–Pt biosensor

The screen-printed DRP550 (Drop Sens) platinum electrodes were cleaned using distilled water. Three biosensor assemblies were prepared for comparing their biosensing efficiency by immobilizing (a) the GOx enzyme onto citrate stabilized gold nanoparticles (Au citrate NPs), (b) GOx onto amino-functionalized gold nanoparticles (Au-amino NPs) and (c) free GOx enzyme directly onto the electrode. Amino functionalization of the working Pt electrodes was achieved by deposition of 10 μl 3-aminopropyltriethoxysilane (3-APS) (5 mM) and incubating it for 2 h in darkness. The electrodes were rinsed with double distilled water to remove unbound 3-APS followed by addition of 10 μl of the cross linking agent (10% (v/v) aqueous solution of glutaraldehyde) that was then air dried. Au-amino NPs were immobilized onto the functionalized electrode surface by dropwise addition. Unbound gold nanoparticles were removed by washing the electrodes 2–3 times with double distilled water. Finally, 20 U of GOx was immobilized onto the electrodes surface coated with Au citrate NPs, Au-amino NPs and directly onto the functionalized electrode surface. The following day, the electrodes were rinsed with water, air dried and stored in PBS (pH 7.4, 0.1 M) at 4 °C for further use.

3. Results and discussion

Gold nanoparticles prepared using the above protocols were characterized by UV–visible absorption spectroscopy, electron microscopy and energy-dispersive X-ray spectroscopy (EDX). The TEM micrographs of the nanoparticles synthesized using trisodium citrate showed spherical gold nanoparticles of average diameter ~18 nm (Fig. 1A). While the nanoparticles synthesized using L-Serine (**Ser**) were of approximately ~20 nm in size, coupled together in a chain like arrangement of particles as shown in Fig. 1B. The amino acid induced covalent coupling, via amide bond formation, among the nanoparticles is clearly demonstrated in the TEM micrographs (Fig. 1C) at higher resolution (300000 × magnification). The amino functionalization on the surface of the nanoparticles is marked by white line surrounding each particle. It can be seen from the TEM micrograph that there is no gap between the individual particles depicting the covalent coupling. These gold nanoparticles were further confirmed through EDX mapping of the electron micrograph shown in Fig. 1D and the corresponding elemental gold mapped as red colored dots.

The observed amino acid induced coupling in electron micrographs was further substantiated by UV–visible spectroscopy. The spectral analysis (Fig. 2) of the synthesized nanoparticles showed a single absorption peak at 523 nm for the citrate stabilized gold nanoparticles (curve a). However, the amino functionalized nanoparticle solution (synthesized using amino acids) showed two absorption peaks for gold nanoparticles – one at 529 nm and a second one at 710 nm (curve b). The double absorption peak is indicative of the anisotropic character of the amino functionalized coupled gold nanoparticles. Here it arises as a result of the coupling among the nanoparticles and formation of chains as observed in the TEM micrographs.

We further examined the electron transfer properties of these synthesized chain like coupled gold nanoparticles. In earlier reports, where such chain like arrangements have been induced with the usage of polymers, the gap between individual particles led to decrease in conductivity (Fang et al., 2008). However, in the present case since there is covalent coupling among the particles, i.e., no gap, hence we expect the conductivity to be affected differently.

3.1. Electrochemical impedance spectroscopy

The electron transfer properties of the synthesized nanoparticles were characterized by electrochemical impedance spectroscopy. Fig. 3 shows the resistance to electron transfer as observed

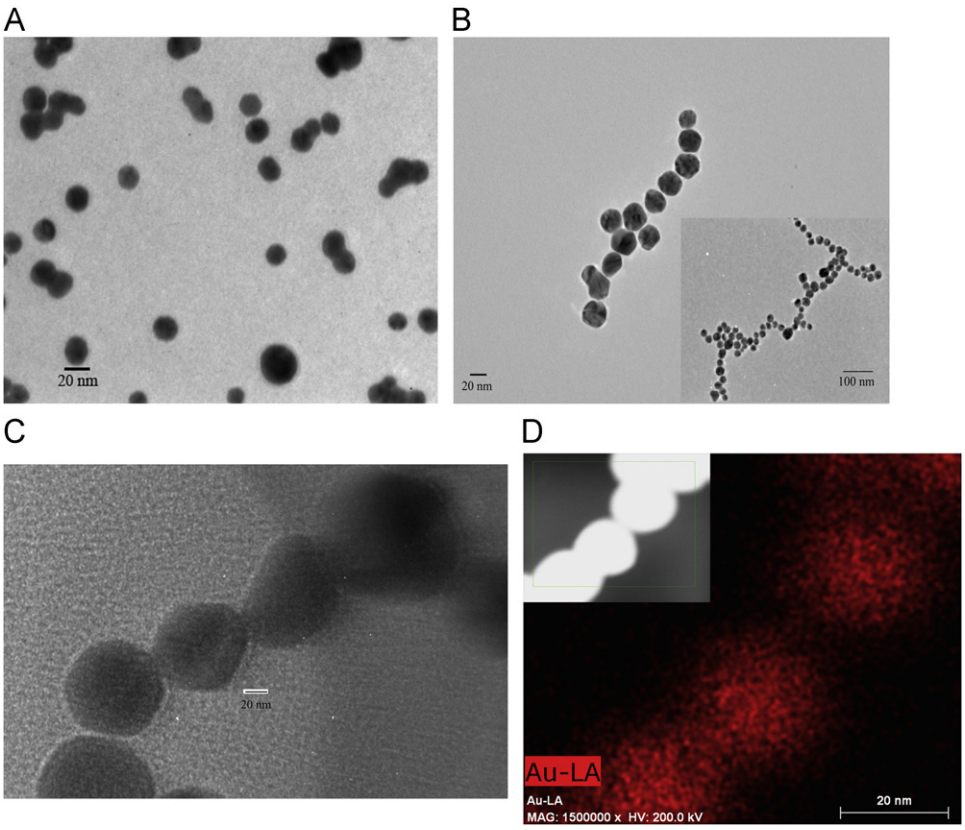

Fig. 1. TEM image of gold nanoparticles using reducing agent (A) trisodium citrate, (B) L-Serine and (C) a higher magnification image of Au amino NPs showing covalent coupling among the particles and (D) EDX of the Au amino NPs.

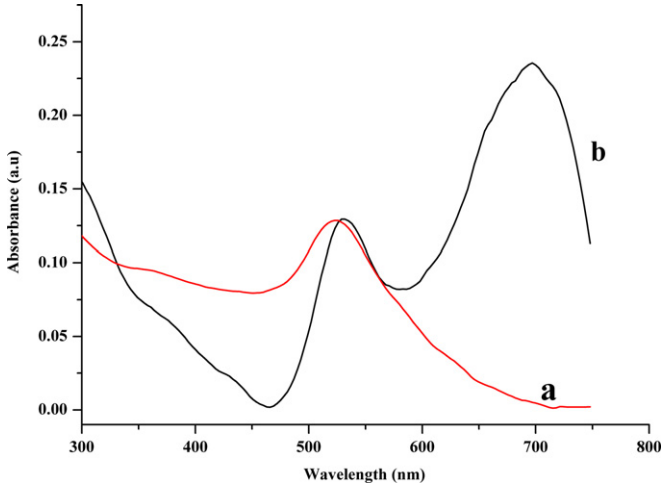

Fig. 2. UV–visible spectra of gold nanoparticles synthesized using (a) tri-sodium citrate (b) L-Serine.

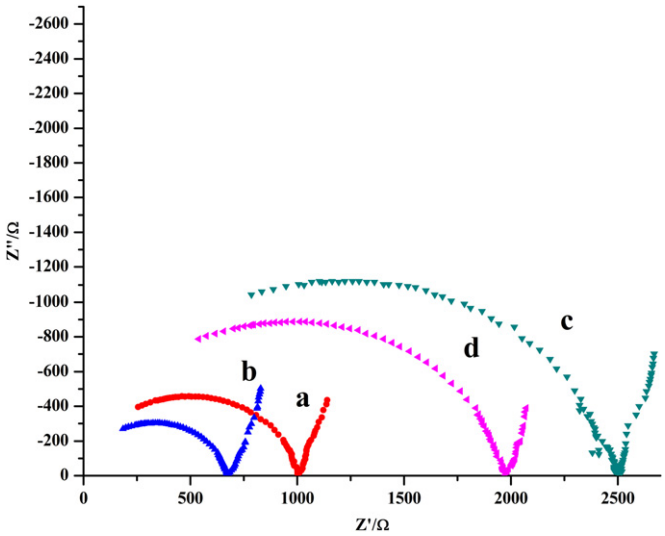

Fig. 3. Cole–Cole plot of EIS for DRP550 electrode modified with (a) Au-citrate NPs (b)Au-amino NPs, (c) GOx–Au-citrate NPs and (d) GOx–Au-amino NPs.

Au-citrate NPs modified electrode (curve a), Au-amino NPs modified electrode (curve b), GOx–Au citrate NPs (curve c) and GOx–Au amino NPs (curve d) modified electrodes. As seen from the graph resistance to electron transfer is least in case of Au-amino NPs modified electrode (678 Ω) and Au-citrate NPs modified electrode showed slightly higher (1014 Ω) resistance while that of bare electrode was 1215 Ω. These results show that modification of electrode surface with gold nanoparticles (Au-citrate NPs and Au-amino NPs) resulted in decrease in electron transfer resistance. However, immobilization of GOx on the electrodes resulted in increased resistance to electron transfer (GOx–Au-citrate NPs 2500 Ω and GOx–Au-amino NPs 1973 Ω) this could be due to the insulator type behavior of the enzyme molecules covering the conducting Au-amino NPs. These results suggest that Au-amino NPs greatly reduces the resistance to electron transfer in comparison to Au-citrate NPs or bare electrode.

3.2. Response characterstics of the fabricated biosensors

Interfacial changes at electrode surface at each stage during fabrication was studied by cyclic voltammograms (CVs). Coating

the working electrode with Au-citrate NPs results in enhancement of background current in comparison to that of bare electrode DRP550 (Fig. S2 in Supplementary Materials) while in case of Au-amino NPs much more enhanced current was observed. This could be attributed to the increased elctroactive surface area in case of NPs modified electrodes as shown by Lu et al. (2007) in case of gold nanowires. As calculated from Randles–Sevcik equation the electroactive surface area in case of chain like Au-amino NPs modified electrode is almost 2 times that of Au-citrate NPs modified electrode implying greater enzyme loading capacity of the former. However, we have kept the enzyme loading constant (20 U of GOx) in each of the electrodes since our aim is to study the effect of chain like coupling of AU-amino NPs on response characteristics of biosensor in comparison to the conventional spherical Au NPs.

GOx immobilized onto Au-amino NPs coated electrode demonstrated redox peaks at a formal potential E^0 of -0.32 V with anodic (E_{PA}) and cathodic peaks (E_{PC}) at -0.38 V and -0.26 V respectively. These peaks could be attributed to the redox conversion at the catalytic site of the GOx enzyme—conversion of GOx–FAD to GOx–$FADH_2$ and vice versa. This suggests an efficient direct electron transfer between the electrode and enzyme catalytic site.

$$GOx\text{–}FAD + 2e^- \leftrightarrow GOx\text{–}FADH_2$$

The influence of scan rate on the fabricated biosensors was evaluated by varying the scan rate from 10 mV to 100 mV for both GOx–Au citrate NP (Fig 4A) and GOx–Au amino NP modified electrodes (Fig. 4B). As seen from inset of Fig 4A and B the peak current (cathodic I_{PC} and anodic I_{PA}) varies linearly with scan rate(υ) rather than $\upsilon^{1/2}$ suggesting that it is not a diffusion controlled process rather a direct electron transfer via a surface controlled electrochemical process. The electron transfer rate constant (k_s) and cathodic transfer coefficient (α) can be calculated from Laviron's equation (Laviron, 1979). Fig. 4C shows plot of E_{PC} and E_{PA} as a function of ln(υ). Cathodic transfer coefficient can be calculated from the slope of the linear fit at high scan rates as

$$E_P = E^0 + RT/\alpha nF - RT\ln(\upsilon)/\alpha nF$$

where R is gas constant, F: Faradays constant, T: temperature and n is number of electron transfer taking place in redox reaction and k_s was calculated from

$$\mathrm{Log}(k_s) = \alpha\log(1-\alpha) + (1-\alpha)\log(\alpha) - \log(RT/nF\alpha) - \alpha(1-\alpha)nF\Delta E_P/(2.303RT)$$

From linear fit of Fig 4C α was estimated from the two slopes corresponding to $2.303\ RT/(1-\alpha)nF$ and $-2.303\ RT/\alpha nF$. The cathodic transfer coefficient for Au-citrate NPs and Au-amino NPs modified electrode was estimated as 0.64 and 0.49 respectively while k_s was found to be 2.4 s^{-1} and 3.12 s^{-1} respectively. As evident from k_s values electron transfer rate is enhanced in case of coupled Au-amino NPs modified electrode as compared to the coventional spherical Au-citrate NPs modified electrode.

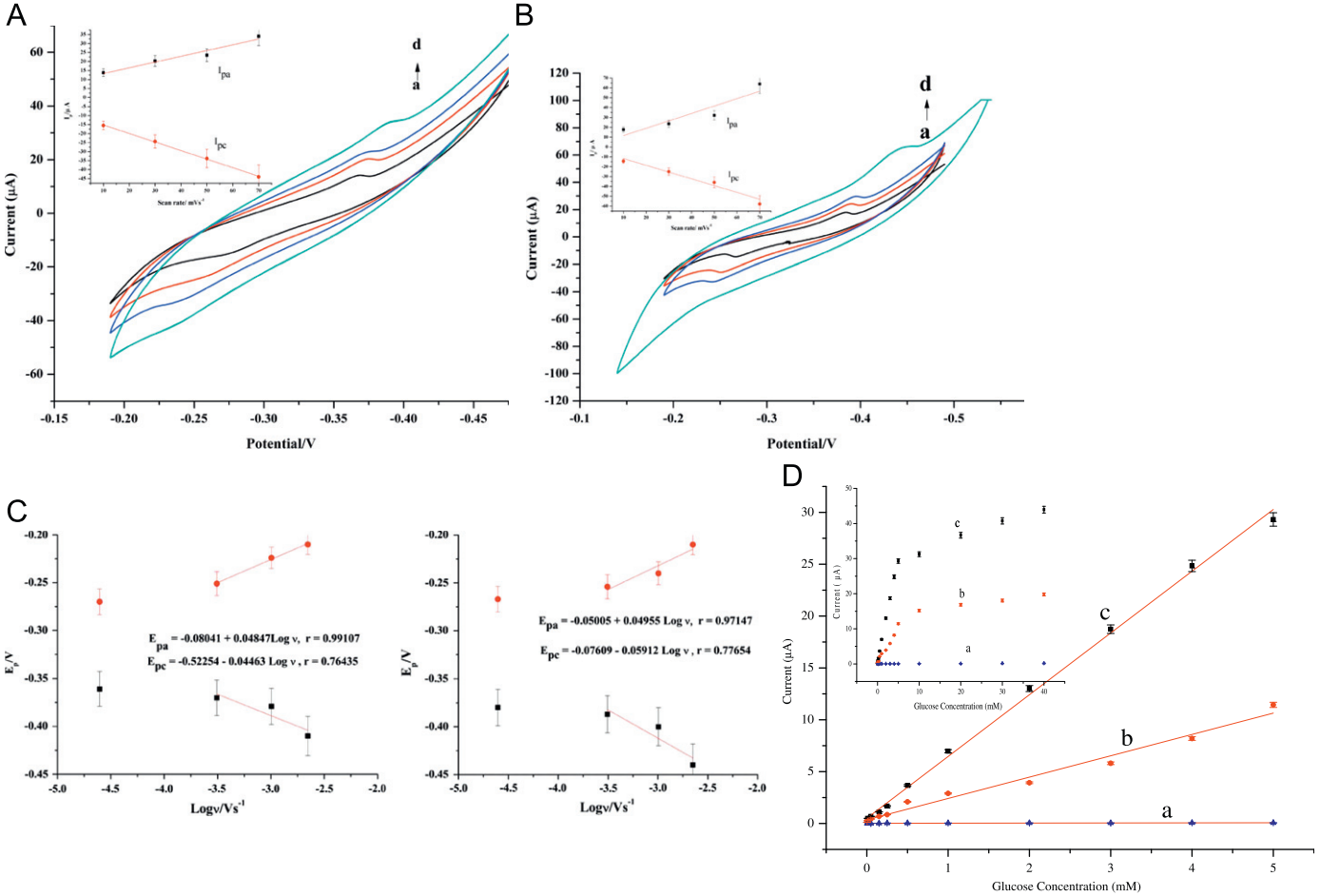

Fig. 4. (A) Cyclic voltammograms of (A) Pt-Au citrate NPs–GOx and (B) Pt-Au amino NPs–GOx for scan rates 0.01, 0.03, 0.05, 0.07 V/s in PBS buffer. Inset shows linear variation of anodic and cathodic peak current. (C) Variation of E_{PC} and E_{PA} with ln(υ) for Pt-Au citrate NPs–GOx (left hand side graph) and Pt-Au amino NPs–GOx (right hand side graph). (D) Calibration plot showing linear behavior of Pt–GOx (curve a), Pt-Au citrate NPs–GOx(curve b) and Pt-Au amino NPs–GOx (curve c) electrodes. Inset shows current response as a function of 1 μM–50 mM glucose concentration.

The *I–V* characteristic of the fabricated biosensors at 1.0 mM glucose concentration is shown in Fig. S3 in Supplementary Materials. A linearly increasing current response was observed up to 0.7 V for all the three biosensors, i.e., GOx (curve a), Gox-Au-citrate NPs (curve b) and GOx-Au-amino NPs (curve c), beyond that voltage saturation in current is observed. Hence 0.7 V was selected as the constant applied voltage for all further measurments. The current response is dependent on concentration of glucose in the sample, applied potential and the pH of the sample. The redox current generated at the electrode is due from direct electron transfer from the redox reaction happening at the GOx catalytic site as discussed above. Moreover, enzyme activity is majorly affected by the pH of the medium. Hence optimization of pH can maximize the current response and hence the sensitivity of the biosensor. (Fig. S4 (A and B) in Supplementary Materials) shows the effect of pH on current response for GOx–Au-citrate NPs and GOx–Au-amino NPs biosensors respectively. Since maximum current was observed at pH 7.0, all further measurements were done at pH 7.0 and 0.7 V applied potential. The current response of the fabricated biosensors as a function of glucose concentration (1.0 μM–40.0 mM) at a constant applied voltage of 0.7 V is shown in Fig. 4D. Water and phosphate buffer (pH 7.0, 0.1 M), taken as negative control, gave zero current response at the applied voltage. The biosensor prepared by direct immobilization of GOx onto the electrode showed much smaller current response in comparison to the other two—GOx–Au amino NPs and GOx–Au citrate NPs biosensors. This is probably due to deactivation of the enzyme leading to lowered activity and hence reduced current response. Moreover, the current response of GOx–Au amino NPs biosensor was almost twice that of GOx–Au-citrate NPs biosensor. The biosensor activity was further analyzed in terms of K_m that serves as an indicator of the enzyme–substrate kinetics (Zeng et al., 2011; Gao et al., 2007). The nonlinear curve fitting of the current response curves of each of the biosensors was done using Michaelis–Menten equation:

$$I = I_{max}\, C/(K_{m,app} + C) \quad (1)$$

where, I and I_{max} represent the current at a given glucose concentration (C) and maximum current respectively, and $K_{m,app}$ is the apparent Michaelis–Menten constant. The values of $K_{m,app}$ and I_{max} from nonlinear fitting was used as guess values for the linear fitting using the Lineweaver–Burk equation:

$$1/I = (K_{m,app}/I_{max})C + 1/I_{max} \quad (2)$$

The $K_{m,app}$ value (Table S1 in Supplementary Materials) for GOx-Au-citrate NPs biosensor was found to be 4.3 mM while that of GOx-Au-amino NPs was 3.11 mM indicating enhanced enzyme activity in the latter case.

Response time was measured as the time taken to record 95% change in concentartion of glucose. The response time of GOx–Au-amino NPs based biosensor was recorded as 4 s while that of GOx–Au-citrate NPs biosensor was 8 s. However, response time of GOx biosensor (without Au NPs) was >15 s. The precision of the biosensor was evaluated by 10 replicates of 1 mM glucose at pH 7.0. Good precision of fabricated biosensors was demonstrated by low RSD value of 1.38% for Au citrate Nps biosensor and 0.84% for Au amino NPs biosensor (Table S1 in Supplementary Materials). The calibration plot showed a linear behavior over 1 μM–5 mM glucose concentrations (as shown in Fig. 4D) beyond which nonlinearity sets in. Table S2 in Supplementary Materials, shows results of linear fit of the fabricated glucose biosensors. GOx–Au amino NPs(curve c) and GOx–Au-citrate NPs(curve b) biosensors showed linear behavior up to 5 mM. However, the GOx biosensor (curve a) has a much lower linear range (up to 0.5 mM). The lower detection limit (in μA range) of the biosensors was recorded as the concentration of glucose below which the observed current is zero. The detection limit of the fabricated GOx–Au-amino NPs biosensor was found to be 1 μM as opposed to 5 μM of GOx–Au-citrate NPs biosensor whereas GOx biosensor could detect only up to 50 μM glucose. In addition to this the sensitivity for the GOx–Au-amino NPs biosensor was much higher (47.2 $\mu A\, mM^{-1}\, cm^{-2}$) as compared to GOx–Au-citrate NPs (16.4 $\mu A\, mM^{-1}\, cm^{-2}$) and GOx (1.21 $\mu A\, mM^{-1} cm^{-2}$) biosensor.

We hypothesize that the observed increased sensitivity and current response is a result of enhanced electron transfer properties of amino-functionalized chain like gold nanoparticles since both the biosensors were fabricated under similar conditions keeping all the parameters constant. Furthermore, this effect can be enhanced by optimizing the concentration of amino acid so as to increase the aspect ratio of the chain like arrangement of nanoparticles (as evident from conductivity analysis).

3.3. Interference and stability analysis

Ascorbic acid (AA) and uric acid (UA) are the major interferants in glucose sensing. We have examined the interference levels of each of these with the Au amino NPs biosensor. The physiological range of AA in humans, ranges between 0.4 and 1.5 mg/dL while that of UA is 2.0–7.0 mg/dL. Ascorbic acid was found to be non-interferring up to 24.6 mg/dL and Uric acid up to 9 mg/dL at the applied voltage of 0.4 V. As evident from the above obeservations, AA and UA both were found to be free from interference for concentration similar to those present in physiological fluids.

The stability analysis of the biosensor was done for more than three months. The sensor was stored at 4 °C in PBS when not in use. Current measurements were done at room temeprature twice a week initially for a month, then every week up to three months. Fig. S5 in Supplementary Materials, shows the relative current data as a function of days of storage. Up to a period of one month the activity loss of the enzymatic electrode was only 10% which decreased further to 15% by end of two months and by end of third month there was $>30\%$ decrease in the performance of the electrode. The operational stability of the fabricated glucose biosensor ($>15\%$ activity till 60 days) is best known till date (see Table 1). This improved stability could be attributed to the biocompatible nature arising from amino functionalization of the nanoparticles (Tiller et al., 2002).

3.4. Probable mechanism of efficient biosensing

The biosensing efficiency is strongly dependent on the properties of the enzyme, in particular, the active site accessibility;

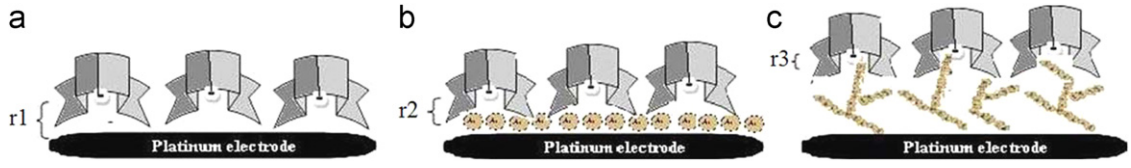

Fig. 5. Schematic representation of approachability of modified electrode surfaces to the buried active center (FAD moiety) of enzyme for diffusion based electron shuttling between FAD and the metal electrode surface (a) without Au particles, (b) with Au citrate NPs and (c) with Au amino NPs.

residues involved in interaction between active site of the enzyme and the carrier molecules attached to the electrode; functional groups on the carrier molecules; shape, size and surface area of the carrier molecules; efficient enzyme immobilization and microenvironment of the elctrode. Normally, the direct electron transfer from Glucose-reduced GOx to metal electrodes is not facilitated because of the appreciably large distance between GOx redox centers and the electrode surface, resulting in a much retarded diffusion controlled electron tranfer rates. As the distance between the acceptor and donor sites increases by 8–17 Å, the rate of electron transfer decreases by 10^4 times. Based on the structure of enzyme, the carrier molecules, current response, response time and conductivity measurements following scheme is proposed for the observed biosensing efficiency of the fabricated biosensors.

Glucose oxidase enzyme is a flavin adenine dinucleotide (FAD) dependent enzyme that catalyzes the oxidation of beta-D-glucose by molecular oxygen. The active center of GOx, i.e., the substrate-binding domain, is buried inside a deep pocket between the two subunits of the dimeric GOx enzyme (see Fig. 5). A cartoon image of the enzyme is used to illustrate the possible biosensing mechanism. Fig. 5 shows schematic representation of the three constructed biosensors. In case (a) where GOx is immobilized directly onto the electrode without any nanoparticles in between, the distance between the active center of GOx (FAD moiety) and the electrode is maximum (r1). However, when GOx is immobilized onto electrode modified using spherical Au citrate NPs particles the enzyme can be immobilized much more efficiently as a result of increased electroactive surface of the nanaoparticles decreasing the distance between the active center and carrier (Au citrate NPs) to r2 (case b). In case of Au amino NPs (chain like nanoparticles) The approachability of chains to the inner core of the active site is much better resulting in further decrease in the distance to r3 (case c). The reduction in the distance results in decreased lengthscales over which diffusion has to take place and in effect reduces the response time. This observation is in conformity with the pioneering work of Heller's group (Degani and Heller., 1987) on direct electrical communication between enzyme and metal electrodes via electron relays.

We think that all the four factors, i.e., decreased distance (hence small response time), enhanced electron transfer rate, amino functionalization and optimum choice of immoblizing agent and its concentration are responsible for enhancing the biosensing efficiency and operational stability. In present case, cumulative effect of all these factors resulted in a much enhanced (approximately three times increase in sensitivity) biosensing efficiency of the GOx–Au amino NPs biosensor as compared to conventional (GOx–Au citrate NPs) biosensor.

4. Conclusions

In this work we have used L-Serine for reduction of $HAuCl_4$ to prepare coupled gold nanoparticles which appear as chains. This coupling among the particles enhances the electron transfer and improves the electrocatalytic property of the biosensor. Moreover, amino functionalization and the chain like structure of the nanoparticles, reduces the response time of the biosensor and improves the operational stability. In addition, it demonstrates better stability and devoid of interference from UA and AA at concentration ranges present in physiological fluids. We feel that the efficiency of the biosensors can be enhanced further by appropriate choice of amino acids and optimization of its concentration. These results indicate that amino acid facilitated gold nanoparticles are potential candidates for electrochemical biosensors with enhanced efficiency, stability and selectivity.

Acknowledgments

This project was funded by All India Council for Technical Education (AICTE) (File no.: 8023/BOR/RID/RPS-68/2008-09). Advanced Instrumentation Research Facility (AIRF), Jawaharlal Nehru University, New Delhi is gratefully acknowledged for TEM work. We are also thankful to Materials Research Laboratory, Sharda University, Noida for allowing us to use the cyclic voltammetry facility and Department of Physics and Material Science and Engineering, JIIT, Noida for impedance spectroscopy. S. Sharma is thankful to JIIT University for providing research fellowship. We would like to acknowledge laboratory technicians Mr. Narendra Kumar Yadav (Biotechnology laboratory) and Mr. Rajneesh Pandey (Electronics laboratory) for the much required help extended by them throughout the work.

Appendix A. Supporting information

Supplementary data associated with this article can be found in the online version at http://dx.doi.org/10.1016/j.bios.2012.04.027.

References

Cao, Z., Zou, Y., Xiang, C., Xian, L., 2007. Analytical Letters 40, 2116–2127.
Chiu, J.Y., Yu, C.M., Yen, M.J., Chen, L.C., 2009. Biosensors and Bioelectronics 24, 2015–2020.
Choi, M.M.F., Pang, W.S.H., Xiao, D., Wu, X., 2001. Analyst 126, 1558–1563.
Clark, L.C., Lyons, C., 1962. Annals of the New York Academy of Sciences 102, 29–35.
Degani, Y., Heller, A., 1987. The Journal of Physical Chemistry 91, 1285–1289.
Fang, C., Fan, Y., Kong, J.M., Gao, Z.Q., Balasubramanian, N., 2008. Applied Physics Letters 92, 263108–263108-3.
Fernandez, R.E., Hareesh, V., Bhattacharya, E., Chadha, A., 2008. Biosensors and Bioelectronics 24, 1276–1280.
Gao, L., Zhuang, J., Nie, L., Zhang, J., Zhang, Y., Gu, N., Wang, T., Feng, J., Yang, D., Perrett, S., Yan, X., 2007. Nature Nanotechnology 2, 577–583.
Laviron, E., 1979. Journal of Electroanalytical Chemistry 101, 19–28.
Liao, C.W., Chou, J.C., Sun, T.P., Hsiung, S.K., Hsieh, J.H., 2007. Sensors and Actuators, B: Chemical 123, 720–726.
Liu, X.Q., Shi, L.H., Niu, W.X., Li, H.J., Xu, G.B., 2008. Biosensors and Bioelectronics 23, 1887–1890.
Lu, J., Drzal, L.T., Worden, R.M., Lee, I., 2007. Chemistry of Materials: a Publication of the American Chemical Society 19, 6240–6246.
Lu, Y., Yang, M., Qu, F., Shen, G., Yu, R., 2007. Bioelectrochemistry (Amsterdam, Netherlands) 71, 211–216.
Majzik, A., Fulop, E., Csapo, E., Bogar, F., Martinek, T., Penke, B., Biro, G., Dekany, I., 2010. Colloids and Surfaces, B: Biointerfaces 81, 235–241.
Mao, X.L., Wu, J., Ying, Y.B., 2008. Chinese Journal of Analytical Chemistry 36, 1749–1755.
Medyantev, E.P., Varlamov, R.M., Gimaletdinov, D.A., Fattakhov, A.N., Budnikov, G.K., 2008. Journal of Analytical Chemistry 63, 3275–3279.
Miao, P., Liang, Z., Liu, L., Chen, G., 2011. Current Nanoscience 7, 354–358.
Nenkova, R., Ivanova, D., Vladimirova, J., Godjevargov., T., 2010. Sensors and Actuators, B: Chemical 148, 59–65.
Nien, P.C., Tung, T.S., Ho, K.C., 2006. Electroanalysis 18, 1408–1415.
Periasamy, A.P., Chang, Y.J., Chen, S.M., 2011. Bioelectrochemistry (Amsterdam, Netherlands) 80, 114–120.
Pmiertu, S., Katrlík, M., Pizzariello, A., Stred'ansk, M., Vital, J., Vorc, J., 1998. Biosensors and Bioelectronics 13, 911–923.
Prabhakar, N., Arora, K., Arya, S., Solanki, P., Iwamoto, M., Singh, H., Malhotra, B.D., 2008. Analyst 133, 1587–1592.
Ren, X., Chen, D., Meng, X., Tang, F., Du, A., Zhang, L., 2009. Colloids and Surfaces, B: Biointerfaces 72, 188–192.
Shan, C.S., Yang, H.F., Song, J.F., Han, D.X., Ivaska, A., Niu, L., 2009. Analytical Chemistry 81, 2378–2382.
Shan, D., Yao, W., Xue, H., 2007. Biosensors and Bioelectronics 23, 432–437.
Shi, W., Ma, Z., 2010. Biosensors and Bioelectronics 26, 1098–1103.
Sun, Y., Wang, H., Sun, C., 2008. Biosensors and Bioelectronics 24, 22–28.
Sun, Y., Yan, F., Yang, W., Sun, C., 2006. Biomaterials 27, 4042–4049.
Tan, Y.N., Lee, J.Y., Wang, D.I.C., 2008. Journal of Physical Chemistry C 112, 5463–5470.
Tiller, J.C., Rieseler, R., Berlin, P., Klemm, D., 2002. Biomacromolecules 3, 1021–1029.

Turkevich, J., Stevenson, P.C., Hillier, J., 1951. Discussions of the Faraday Society 11, 55–75.
Wang, T., Cook, C., Derby, B., 2009. IEEE Xplore, 82–85.
Wang, X., Zhang, Y., Banks, C.E., Chen, Q., Ji, X., 2010. Colloids and Surfaces, B: Biointerfaces 78, 363–366.
Wu, H., Wang, J., Kang, X., Wang, C., Wang, D., Liu, J., Aksay, I.A., Lin, Y., 2009. Talanta 80, 403–406.
Zeng, Q., Cheng, J.S., Liu, X.F., Bai, H.T., Jiang, J.H., 2011. Biosensors and Bioelectronics 26, 3456–3463.
Zhang, F.F., Wan, Q., Wang, X.L., Sun, Z.D., Zhu, Z.Q., Xian, Y.Z., Jin, L.T., Yamamoto, K., 2004. Journal of Electroanalytical Chemistry 571, 133–138.
Zuo, S., Teng, Y., Yuan, H., Lan, M., 2008. Sensors and Actuators, B: Chemical 133, 555–560.